In Situ Investigation of the Thermal Decomposition of Ammonium Tetrathiomolybdate Using Combined Time-Resolved X-ray Absorption Spectroscopy and X-ray Diffraction

Richard I. Walton,[†] Andrew J. Dent,[‡] and Simon J. Hibble*[,†]

Department of Chemistry, The University of Reading, Whiteknights, Reading RG2 2AD, U.K., and CLRC Daresbury Laboratory, Daresbury, Warrington WA4 4AD, U.K.

Received August 4, 1998. Revised Manuscript Received August 4, 1998

The thermal decomposition of ammonium tetrathiomolybdate, a process widely used for the preparation of molybdenum sulfides, has been studied in situ for the first time, using combined Mo K edge XAFS and X-ray powder diffraction. Isothermal decomposition at 120 °C produced pure amorphous molybdenum trisulfide (*a*-MoS_3), after 135 min, with no further reaction observed on continued heating. XAFS spectra and diffraction patterns collected during the heating showed the disappearance of crystalline $(NH_4)_2MoS_4$ and the formation of *a*-MoS_3 without the formation of an intermediate. Thermal decomposition of $(NH_4)_2MoS_4$ by heating from 100 to 400 °C produced ultimately poorly crystalline MoS_2. It is shown that the Mo−Mo nonbonded correlation of ∼3.2 Å found by some previous workers in *a*-MoS_3 is most likely due to the presence of small quantities of poorly crystalline MoS_2. This allows certain structural models for *a*-MoS_3 to be ruled out. A detailed comparison between XAFS data collected from crystalline 2H−MoS_2 at a variety of temperatures and data collected from poorly crystalline MoS_2 prepared in situ shows that the low crystallinity exhibited by the powder pattern of the latter material arises from not only small particle size and stacking faults but also positional disorder of constituent atoms from the ideal 2H−MoS_2 structure.

Introduction

Molybdenum sulfides are of great industrial importance. For many years crystalline molybdenum disulfide, MoS_2, has been the basis of hydrotreating catalysts, vital for the purification of petroleum products.[1] It is widely accepted, for example, that the catalytically active species in hydrodesulfurization processes are MoS_2 crystallites, formed by the sulfidation of the Mo/Al_2O_3/Co catalyst under operating conditions.[2,3] Crystalline molybdenum disulfide also finds uses as a lubricant either in a solid form or as an additive in liquid systems,[4] and an amorphous material of composition MoS_2 has been investigated as a cathode material for reversible nonaqueous lithium batteries.[5] Amorphous molybdenum trisulfide, *a*-MoS_3, has shown greater potential in this area of electrochemistry, exhibiting unusually high energy-density and reversibility when compared to crystalline transition-metal sulfides.[6,7]

The thermal decomposition of ammonium tetrathiomolybdate under an inert gas atmosphere offers a convenient method for the preparation of binary molybdenum sulfides and utilizes lower temperature than other preparative routes, such as the sulfidation of molybdenum oxides. The process may be represented as

$$(NH_4)_2MoS_4 = a\text{-}MoS_3 + 2NH_3 + H_2S = MoS_2 + S$$

This reaction was first described by Berzelius in the 1830's,[8] and the products of each stage of the process have since been the subject of numerous investigations, using methods such as X-ray diffraction,[9] thermogravimetric and differential thermogravimetric analysis,[10−12] and electrical conductivity measurements.[13] It is understood from these experiments that ammonium tetrathiomolybdate produces *a*-MoS_3 when heated at

* Author for correspondence. E-mail s.j.hibble@rdg.ac.uk.
[†] University of Reading.
[‡] CLRC Daresbury Laboratory.

(1) Prins, R.; De Beer, V. H. J.; Somorjai, G. A. *Catal. Rev.−Sci. Eng.* **1989**, *31*, 1.
(2) Muijsers, J. C.; Weber, T.; van Hardeveld, R. M.; Zandbergen, H. W. *J. Catal.* **1995**, *157*, 698.
(3) Weber, T.; Muijsers, J. C.; van Wolpot, J. H. M. C.; Verhagen, C. P. J.; Niemantsverdriet, J. W. *J. Phys. Chem.* **1996**, *100*, 14144.
(4) Miremadi, B. K.; Colbow, K.; Morrison, S. R. *J. Appl. Phys.* **1997**, *82*, 2639, and references cited therein.
(5) Jacobson, A. J.; Chianelli, R. R.; Whittingham, M. S. *J. Electrochem. Soc.* **1979**, *120*, 2277.
(6) Jacobson, A. J.; Chianelli, R. R.; Rich, S. M.; Whittingham, M. S. *Mater. Res. Bull.* **1979**, *14*, 1437.
(7) Auborn, J. J.; Barberio, Y. L.; Hanson, K. J.; Schleich, D. M.; Martin, M. J. *J. Electrochem. Soc.* **1987**, *134*, 581.
(8) Berzelius, J. J. *Traité de Chimie*; Firman Didot Frères: Paris, 1830.
(9) Wildervanck, J. C.; Jellinek, F. *Z. Anorg. Allg. Chem.* **1964**, *328*, 309.
(10) Prasad, T. P.; Diemann, E.; Müller, A. *J. Inorg. Nucl. Chem.* **1973**, *35*, 1895.
(11) Nirsha, B. M.; Savel'eva, L. V.; Rekharskii, V. I. *Inorg. Mater.* **1985**, *21*, 325.
(12) Brito, J. L.; Ilija, M.; Hernández, D. *Thermochim. Acta* **1997**, *256*, 325.
(13) Belougne, P.; Bensimon, Y.; Deriode, B.; Giuntini, J. C.; Zanchetta, J. V. *Philos. Mag. B* **1993**, *67*, 215.

10.1021/cm980716h CCC: $15.00
Published on Web 10/13/1998

temperatures between 120 and 260 °C under either vacuum or an inert atmosphere. Amorphous MoS_3 is stable to around 300 °C, when gradual loss of sulfur produces ultimately MoS_2 at around 400 °C. Temperatures in excess of 1000 °C result in the formation of solely hexagonal molybdenum disulfide (2H−MoS_2). As has previously been noted, the precise temperatures representing each of these steps shows some variation among the different published studies, which is most likely due to differing reaction conditions, in particular the heating rates applied.[12]

The molybdenum disulfide produced by heating ammonium tetrathiomolybdate to 400 °C exists in a poorly crystalline modification, shown by some workers to be structurally related to crystalline 2H−MoS_2 on the basis of X-ray diffraction results.[9,14] The catalytic properties of this disordered phase have recently been investigated, and it has been shown that the thermal decomposition of ammonium tetrathiomolybdate affords molybdenum disulfide with a considerably higher catalytic activity toward hydrogenation reactions than sulfides prepared by conventional methods, such as the reductive sulfidation of oxides.[15,16] The process has also been investigated recently as a means of modifying the tribological properties of aluminum surfaces: the electrochemical deposition of *a*-MoS_3 from ammonium tetrathiomolybdate on aluminum surfaces followed by heat treatment around 400 °C has been used to produce aluminum surface-impregnated with MoS_2 that has improved wear properties.[17−19]

Amorphous molybdenum trisulfide, the initial decomposition product of ammonium tetrathiomolybdate, is one of a number of unusual transition-metal sulfides which has no crystalline analogue; other examples include V_2S_5,[20] WS_3,[21] and Re_2S_7.[22] The structures of these compounds have been the subject of widespread speculation in the literature,[23] and *a*-MoS_3 in particular has been the subject of numerous structural investigations but without any consensus on even a simple structural building block to describe its structure having been reached. The most widely assumed structural model for *a*-MoS_3 is based on the chainlike structures of the crystalline transition-metal trichalcogenides of groups 4 and 5, with metal−metal bonded molybdenum dimers bridged by sulfide and disulfide anions, resulting in the compound being formulated as $Mo^{V}(S_2^{2-})_{0.5}(S^{2-})_2$. This model arose from a comprehensive EXAFS and X-ray diffraction study of the compound by Liang and co-workers in the 1980s,[24−27] who confirmed the earlier conclusions of Diemann,[28] who first showed MoS_3 to be a genuine compound rather than a mixture of amorphous forms of MoS_2 and sulfur. The basis of the chain model is an Mo_2S_9 unit, Figure 1a. Molybdenum is surrounded by six sulfur near neighbors (d(Mo−S) = 2.43 Å) and alternating short (2.75 Å) and long (~ 3.20 Å) Mo−Mo distances are produced when units are linked by face sharing of the terminal S atoms to form an infinite chain. Other EXAFS studies of *a*-MoS_3 show general agreement with this model,[29−31] and our recent neutron diffraction study favors such a chain model over other possibilities, particularly those containing multinuclear Mo−Mo bonded clusters.[32] In recent years, however, Müller and co-workers have put forward a second model for the structure of *a*-MoS_3, in which Mo−Mo bonded triangular clusters are linked by bridging disulfide and monosulfide anions, Figure 1b. This model was proposed on the basis of results of chemical degradation experiments in which *a*-MoS_3 was reacted with aqueous solutions of cyanide or hydroxide at ambient temperature to produce crystalline complexes containing multinuclear Mo−Mo bonded clusters such as $[Mo_3S_4(CN)_9]^{5-}$,[33] $[Mo_4S_4(CN)_{12}]^{8-}$,[33] and $[Mo_3S_{13}]^{2-}$.[34,35]

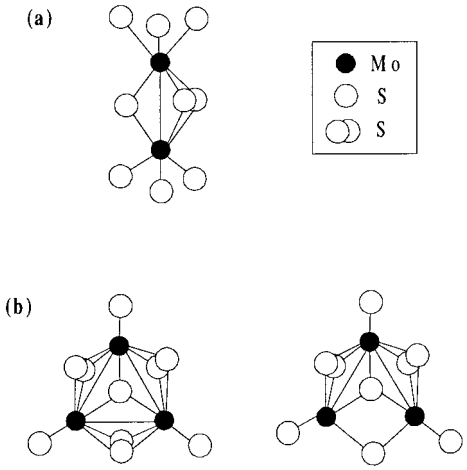

Figure 1. Two structural models previously proposed for *a*-MoS_3: (a) an $Mo^{V}_2S_9$ unit that may form part of an infinite MoS_3 chain by face sharing of terminal S groups (d(Mo−Mo) = 2.75 Å); (b) two of the trinuclear clusters containing Mo^{IV} proposed by Weber et al. as structural units.[36] Such clusters are linked to others by appropriate amounts of charge balancing S^{2-} and S_2^{2-} groups; two possible units are shown, one with d(Mo−Mo) = 2.80 Å and the other with d(Mo−Mo) = 2.75 Å and d(Mo−Mo)′ = 3 Å. Bold lines represent Mo−Mo bonds (d(Mo−Mo) < 3 Å).

(14) Liang, K. C.; Chianelli, R. R.; Chien, F. Z.; Moss, S. C. *J. Non-Cryst. Solids* **1986**, *79*, 251.
(15) Vasudevan, P. T.; Zhang, F. *Appl. Catal., A: Gen.* **1994**, *112*, 161.
(16) Zhang, F.; Vasudevan, P. T. *J. Catal.* **1995**, *157*, 536.
(17) Wang, H. W.; Skeldon, P.; Thompson, G. E.; Wood, G. C. *J. Mater. Sci. Lett.* **1996**, *15*, 494.
(18) Wang, H. W.; Skeldon, P.; Thompson, G. E.; Wood, G. C. *J. Mater. Sci.* **1997**, *32*, 497.
(19) Skeldon, P.; Wang, H. W.; Thompson, G. E. *Wear* **1997**, *206*, 187.
(20) Diemann, E.; Müller, A. *Z. Anorg. Allg. Chem.* **1978**, *444*, 181.
(21) Tsigdinos, G. A. *Top. Curr. Chem.* **1978**, *76*, 65.
(22) Hibble, S. J.; Walton, R. I. *J. Chem. Soc., Chem. Commun.* **1996**, 2135.
(23) Chianelli, R. R *Int. Rev. Phys. Chem.* **1982**, *2*, 127.
(24) Liang, K. S.; de Neufville, J. P.; Jacobson, A. J.; Chianelli, R. R. *J. Non-Cryst. Solids* **1980**, *35*, 1249.
(25) Liang, K. S.; Cramer, S. P.; Johnston, D. C.; Chang, C. H.; Jacobson, A. J.; de Neufville, J. P.; Chianelli, R. R. *J. Non-Cryst. Solids* **1980**, *42*, 345.
(26) Cramer, S. P.; Liang, K. S.; Jacobson, A. J.; Chang, C. H.; Chianelli, R. R. *Inorg. Chem.* **1984**, *23*, 1215.
(27) Chien, F. Z.; Moss, S. C.; Liang, K. S.; Chianelli, R. R. *Phys. Rev. B* **1984**, *29*, 4606.
(28) Diemann, E. *Z. Anorg. Allg. Chem.* **1977**, *432*, 127.
(29) Huntley, D. R.; Parham, T. R.; Merrill R. P.; Sienko M. J. *Inorg. Chem.* **1983**, *26*, 4144.
(30) Scott, R. R.; Jacobson, A. J.; Chianelli, R. R.; Pan, W.-H.; Stiefel, E. I.; Hodgson K. O.; Cramer, S. P. *Inorg. Chem.* **1986**, *25*, 1461.
(31) Hibble, S. J.; Rice, D. A.; Pickup, D. M.; Beer, M. P. *Inorg. Chem.* **1995**, *34*, 5109.
(32) Hibble, S. J.; Walton, R. I.; Pickup, D. M.; Hannon, A. C. *J. Non-Cryst. Solids* **1998**, *232−234*, 434.
(33) Müller, A.; Jostes, R.; Eltzner, W.; Chong-Sei, N.; Diemann, E.; Bögge, H.; Zimmermann, M.; Dartmann, M.; Reinsch-Vogell, V.; Shun, C.; Cyvin, S. J.; Cyvin, B. N. *Inorg. Chem.* **1985**, *24*, 2872.
(34) Müller, A.; Fedin, V.; Hegetschweiler, K.; Amrein, W. *J. Chem. Soc., Chem. Commun.* **1992**, 1795.

It was suggested that the Mo^{IV}_3 core found in some of these complexes forms a building block for the structure of *a*-MoS_3 with charge-balancing S^{2-} and S_2^{2-} anions.[34,35] Most recently Weber et al. performed a chemical degradation experiment on *a*-MoS_3 using NEt_4Cl, producing the complex $(NEt_4)_2[Mo_3S_7Cl_6]$ containing the Mo^{IV}_3 triangular core.[36] These authors produce a more detailed description of a possible structure of *a*-MoS_3, suggesting that two types of trinuclear Mo $^{IV}_3$ cluster are present in the material, one with three equal Mo−Mo bonding distances of ∼2.7 Å and another with short (∼2.7 Å) and long (∼3. Å) Mo−Mo interactions, as shown in Figure 1b. Clearly these most recent descriptions of the structure of *a*-MoS_3 show little consistency with the earlier studies which took information directly from the solid state. It is noteworthy that the use of photoelectron spectroscopy in determining the oxidation state of Mo in *a*-MoS_3 has not allowed possible units to be distinguished: some authors claim the compound contains solely Mo^{V} [24,25] and others Mo^{IV}.[36,37] We considered a reexamination of the structure of *a*-MoS_3 to be worthwhile, using an experimental technique not previously applied to the system.

In this paper we describe the first in situ structural study of the thermal decomposition of ammonium tetrathiomolybdate using combined XAFS/XRD. The method has been shown to be a powerful tool for the study of solid-state transformations under various conditions, allowing both long-range order and short-range order to be examined simultaneously.[38−40] The aims of the experiment were to gain new information about the structure of *a*-MoS_3 and to examine the local structure of poorly crystalline MoS_2, a material clearly of widespread interest at present.

Experimental Section

Materials. Ammonium tetrathiomolybdate was used as supplied by Aldrich (99.9%). An infrared spectrum of this material showed no oxide impurities were present, by the absence of any characteristic Mo−O vibrations. Crystalline (2H) molybdenum disulfide, used as a model compound for the EXAFS experiments, was used as supplied by Aldrich.

XAFS/XRD Experiment. Combined XAFS/XRD experiments were performed on Station 9.3 of the Daresbury SRS using experimental apparatus previously described.[38−40] The synchrotron source was operating with an average stored energy of 2 GeV and a typical electron current of 200 mA. EXAFS data were collected at the molybdenum K edge ($E \approx$ 20 000 eV) in transmission mode from samples of ammonium tetrathiomolybdate and crystalline molybdenum disulfide finely ground with boron nitride as a diluent and pressed into 13 mm diameter pellets of around 1 mm thickness. A diluent was necessary to prevent cracking of the thin pellets upon heating with the release of the gaseous byproducts in the decomposition of ammonium tetrathiomolybdate and also to allow the sample concentration to be adjusted to prevent self-absorption ($\mu d \approx 2.5$, $\Delta\mu d \approx 1$). Boron nitride was found to be suitable for this purpose since its powder diffraction pattern contains only a small number of well-defined Bragg peaks, few of which overlap with those of either ammonium tetrathiomolybdate or molybdenum disulfide, and over the temperature range studied here it undergoes no phase change and is unreactive toward the materials studied. Typically pellets containing ∼50% by mass of sample were used. EXAFS data were collected in quick-EXAFS mode using a rapidly scanning Si(220) monochromator, with the maximum *k*-value of the data limited to 16 $Å^{-1}$; this range of data was sufficient to allow detailed modeling of several atomic shells but minimized the cycle time of the experiment. EXAFS data were calibrated using data collected from a molybdenum foil. Powder X-ray diffraction data were collected alternately with the EXAFS data using an X-ray wavelength of 1.2 Å, slightly lower in energy than the molybdenum K edge, for a period slightly less than 5 min over the range $2\theta \approx 14-72°$. Diffraction patterns were collected using an INEL curved, position-sensitive detector which was calibrated using a silicon standard. The combined time for an EXAFS scan, collection of an XRD pattern, and associated monochromator movement time was 10 min. Station 9.3 is equipped with a furnace which allows solid samples to be heated to 1000 °C, and the temperature of the sample may be measured to within ±2 °C, using a thermocouple positioned on the sample surface. Two experiments were performed on ammonium tetrathiomolybdate, both under an atmosphere of flowing dry nitrogen. In the first a sample was heated rapidly (20 °C min^{-1}) to 120 °C, the lowest temperature reported for the onset of decomposition of the compound;[12] then EXAFS and XRD data were collected with the temperature maintained at this level for 4 h. In the second experiment a sample was heated rapidly to 100 °C at 20 °C min^{-1} and then heated at 1 °C min^{-1}, while EXAFS and XRD data were measured until the temperature had reached 400 °C. Data were measured from crystalline MoS_2 diluted in boron nitride at a variety of temperatures between room temperature and 400 °C to provide a direct comparison for the data collected from the decomposition products of ammonium tetrathiomolybdate.

Data Analysis. EXAFS data calibration and background subtraction were performed using the programs EXCALIB and EXBACK and data modeled in *k*-space with k^3-weighting from $k = 3$ $Å^{-1}$ to $k = 16$ $Å^{-1}$ using the program EXCURV92.[41] For each EXAFS spectrum analyzed the threshold energy was defined as the point of inflection of the near-edge region, and a postedge background calculated using a combination of three third-order polynomials. Phase shifts were calculated within EXCURV92 using the Hedin−Lundqvist method for determining ground-state potentials and the von Barth method for exchange potentials. EXAFS spectra were Fourier transformed to produce a one-dimensional radial distribution function, using phase shifts calculated for the first atomic shell.

Elemental Analysis. The pellets used in the EXAFS/XRD experiment were retained after heat treatment and finely ground. X-ray microanalysis was performed using a Philips CM20 transmission electron microscope fitted with an EDAX PV9900 detection unit and operating with an accelerating voltage of 200 keV. This allowed the examination of particles containing only molybdenum and sulfur without interference from the diluent boron nitride. A calibration graph was derived from study of the Mo−L, Mo−K, and S−K emissions of crystalline MoS_2, $(NH_4)_2MoS_4$, and MoO_3 to convert the ratio of observed X-ray emission intensities to relative atomic concentrations.[31] Typically 10 metal sulfide particles in each mixture were analyzed in this way.

Results and Discussion

Decomposition of Ammonium Tetrathiomolybdate at 120 °C. Figure 2 shows the X-ray powder

(35) Müller, A.; Diemann, E.; Krickemeyer, E.; Walberg, H.-J.; Bögge, H.; Armatage, A. *Eur. J. Solid State Inorg. Chem.* **1993**, *30*, 565.

(36) Weber, Th.; Muijsers, J. C.; Niemantsverdriet, J. W. *J. Phys. Chem.* **1995**, *99*, 9194.

(37) Khudorozhko, G. F.; Asanov, I. P.; Mazalov, E. A. Kravtsova, G. K.; Parygina, G. K.; Fedorov, V. E.; Minorov, J. V. *J. Electron Spectrosc. Related Phenom.* **1994**, *68*, 199.

(38) Couves, J. W.; Thomas, J. M.; Waller, D.; Jones, R. H.; Dent, A. J.; Greaves, G. N. *Nature* **1991**, *345*, 465.

(39) Sankar, G.; Wright, P. A.; Natarajan, S.; Thomas, J. M.; Greaves, G. N.; Dent, A. J.; Dobson, B. R.; Ramsdale, C. A.; Jones, R. H. *J. Phys. Chem.* **1993**, *97*, 9550.

(40) Epple, M.; Sankar, G.; Thomas, J. M. *Chem. Mater.* **1997**, *9*, 3127.

(41) Binstead, N.; Campbell, J. W.; Gurman, S. J.; Stephenson, P. C. *EXCURV92*; SERC Daresbury Laboratory: Daresbury, U.K., 1991.

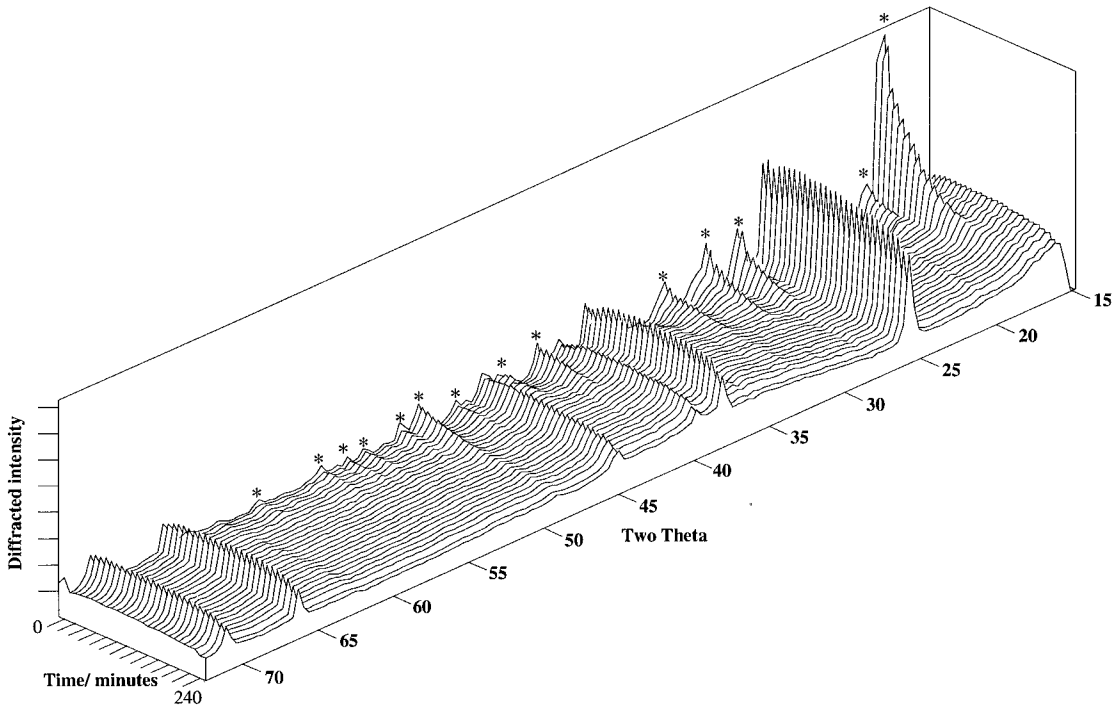

Figure 2. Powder diffraction patterns recorded during the isothermal heating of ammonium tetrathiomolybdate at 120 °C. Each pattern was obtained during a period of 5 min. Bragg peaks due to $(NH_4)_2MoS_4$ are marked with an asterisk; other Bragg peaks are due to the diluent boron nitride.

diffraction patterns recorded as ammonium tetrathiomolybate was held at 120 °C for 4 h. Bragg peaks due to crystalline $(NH_4)_2MoS_4$ decrease in intensity with time, most clearly indicated by the magnitude of the (202) peak at ∼18°, and after 135 min there remains no trace of the starting material; the only Bragg peaks present for the remainder of the heating are due to the diluent boron nitride, consistent with the presence of only *a*-MoS_3 under these conditions. Elemental analysis of the product of this reaction showed the molybdenum sulfide produced has composition $MoS_{3.1(1)}$.

Analysis of the Mo K edge EXAFS of ammonium tetrathiomolybdate at 120 °C recorded in the first 5 min of heating showed that only one shell of atoms is required to model the data, those associated with the MoS_4^{2-} anion, Figure 3a. On least-squares refinement of the coordination number, radial distance, and Debye−Waller factor, a satisfactory fit is achieved with physically reasonable structural parameters. The EXAFS derived Mo−S distance (2.18 Å, Table 1) is in excellent agreement with that determined from a previous crystallographic study of the compound (2.17 Å).[42] The second EXAFS spectrum, recorded during 10−15 min of heating, showed changes had already occurred in the average local structure of molybdenum. These were most evident in the Fourier transform which showed a broadening of the single peak to give a less symmetrical feature in the radial distribution function. Table 1 shows that three shells of atoms are necessary to model these data well; inclusion of a second sulfur shell at ∼2.43 Å and a molybdenum shell at ∼2.75 Å produce a satisfactory fit to the data. The result of including occupation numbers of these shells in least-squares refinements is reported in Table 1 (it was always checked that the number of independent parameters, N_{ind}, and the distance resolution, Δr, were within limits determined using standard expressions for EXAFS data analysis when performing least-squares refinements[43]). The EXAFS data of the sample after 15 min of heating may be interpreted as arising simply from a mixture of ammonium tetrathiomolybdate and *a*-MoS_3. Previous EXAFS studies of *a*-MoS_3 all find molybdenum to be surrounded by six near sulfur neighbors at 2.41−2.44 Å and to have at least one molybdenum neighbor at 2.74−2.75 Å.[24−31] For a mixture consisting of 25% MoS_3 and 75% $(NH_4)_2MoS_4$ we would expect each molybdenum to be surrounded by, on average, 3 sulfur neighbors at ∼2.17 Å, 1.25 sulfur neighbors at 2.43 Å, and at least 0.25 molybdenum neighbors at 2.75 Å. The coordination numbers derived from the EXAFS data collected during 10−15 min of heating ammonium tetrathiomolybdate at 120 °C are consistent with these data, bearing in mind the large expected errors on EXAFS derived coordination numbers. As time proceeds, the EXAFS data may be modeled in exactly the same manner, as simple mixtures of ammonium tetrathiomolybdate and *a*-MoS_3, but with increasing amounts of *a*-MoS_3 in the mixture, indicated by smaller contributions of the sulfur shell at 2.18 Å and increasingly larger contributions of the sulfur shell at 2.43 Å and the molybdenum shell at 2.76 Å. Figure 3b shows the EXAFS spectrum and its Fourier transform for the period of 30−35 min of heating, clearly illustrating the dramatic changes in the data seen during the thermal decomposition. Another indication of the decay of ammonium tetrathiomolybdate is shown by changes in the near-edge structure (XANES) of the Mo K edge as time proceeds. Figure 4

(42) Belounge, P.; Chezeau N.; Lapasset, J. *Acta Crystallogr. B* **1976**, *32*, 3087.

(43) *Report on the International Workshops on Standards and Criteria in XAFS* in *X-ray Absorption Fine Strucure*; Hasnain, S. S., Ed.; Ellis Horwood: Chichester, U.K., 1991.

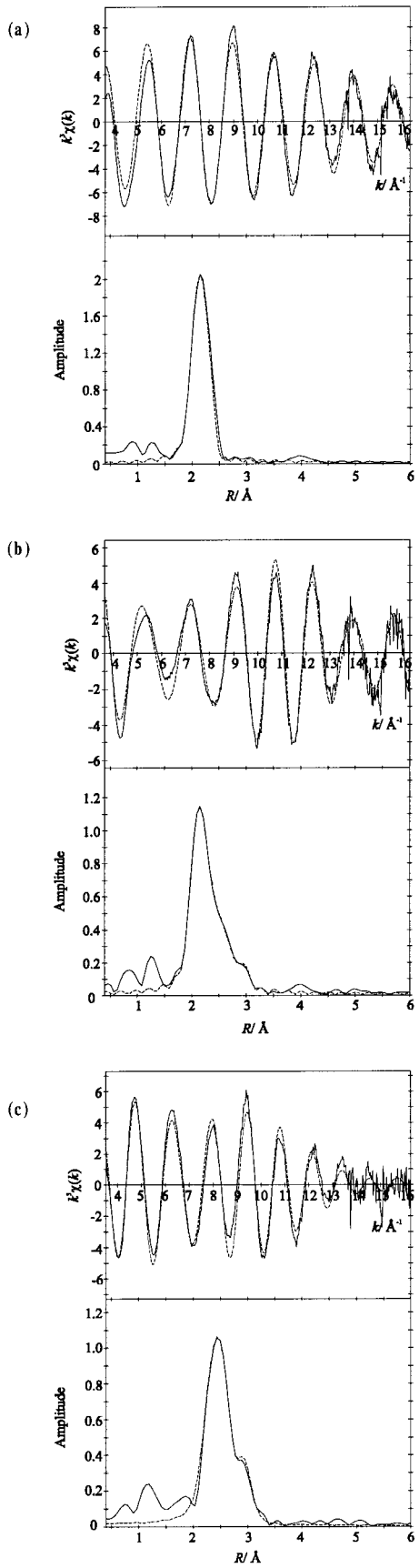

Figure 3. Mo K edge EXAFS spectra (top) and their Fourier transforms (bottom) recorded during the isothermal heating of ammonium tetrathiomolybdate at 120 °C, recorded at (a) 0−5, (b) 30−35, and (c) 130−135 min. Broken lines show the theoretical functions generated from models fitted to the data (see Table 1).

Table 1. Structural Parameters Derived from Study of the Mo K Edge EXAFS Obtained during the Isothermal Decomposition of $(NH_4)_2MoS_4$ at 120 °C at Selected Times

time/min	shell	*N*	*R*/Å	*A*/Å^2	fit index
0−5	S	4.00(9)	2.179(1)	0.0047(2)	2.19
10−15	S	3.94(13)	2.182(2)	0.0057(3)	2.24
	S	1.61(45)	2.449(6)	0.0133(42)	
	Mo	0.29(18)	2.760(10)	0.0087(45)	
30−35	S	2.81(9)	2.183(1)	0.0053(4)	2.69
	S	3.10(30)	2.428(2)	0.0157(19)	
	Mo	0.47(10)	2.762(3)	0.0057(14)	
60−65	S	1.92(12)	2.187(2)	0.0074(7)	4.54
	S	4.69(21)	2.427(2)	0.0149(10)	
	Mo	0.95(14)	2.764(3)	0.0096(11)	
90−95	S	0.91(12)	2.183(3)	0.0058(11)	2.90
	S	5.57(19)	2.427(3)	0.0160(8)	
	Mo	1.16(13)	2.765(2)	0.0094(9)	
130−135	S	6.64(16)	2.430(2)	0.0156(5)	1.96
	Mo	1.38(13)	2.766(2)	0.0096(8)	

[a] Estimated errors are those derived from least-squares fitting procedures and take no account of experimental error. *N* is the shell occupation number, *R* its radial distance, and *A* its Debye−Waller Factor ($=2\sigma^2$). The fit index is defined as $\sum(k^3(\chi_i^{calc}(k) - \chi_i^{exp}(k)))^2$, where $\chi_i^{calc}(k)$ and $\chi_i^{exp}(k)$ are the *i*th data points of the calculated and experimental X-ray absorption coefficients, respectively.

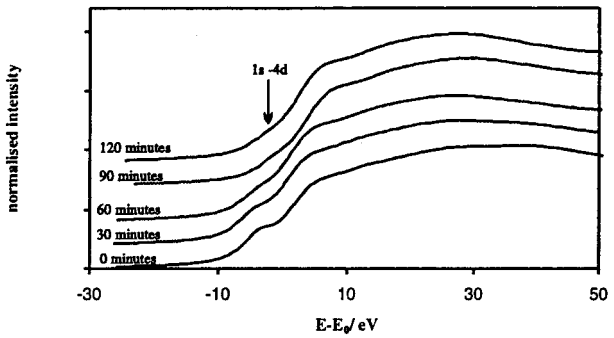

Figure 4. Normalized Mo K edge XANES spectra recorded during the heating of ammonium tetrathiomolybdate at 120 °C, offset for clarity. The preedge 1s−4d transition, characteristic of a tetrahedrally coordinated center, is indicated.

shows the Mo K edge XANES at four different times. It can be seen that the preedge feature, characteristic of a tetrahedrally coordinated center, decreases in intensity as the tetrahedral MoS_4^{2-} anion decays to produce MoS_3, containing six-coordinate molybdenum. After 130−135 min of heating the EXAFS data are best modeled by two atomic shells; corresponding to the previously determined EXAFS parameters for *a*-MoS_3, Figure 3c, Table 1. During continued heating there results no change in the EXAFS data; data collected after 8 h is best modeled in exactly the same manner as those collected after 135 min.

The thermal decay of ammonium tetrathiomolybdate may be represented graphically using both the EXAFS and XRD results. Figure 5a shows plots of the fractional amount of $(NH_4)_2MoS_4$ derived from the average coordination number of the shell of sulfur atoms at 2.18 Å (derived from EXAFS and associated with the tetrathiomolybdate anion), and the normalized intensity of the (202) (2θ = 18.3°) and (115) (2θ = 30.8°) peaks of ammonium tetrathiomolybdate (XRD) as a function of time. The coordination numbers were determined by least-squares refinement of parameters of three atomic shells as described above, and the Bragg peak intensity was determined by fitting a Gaussian function to the

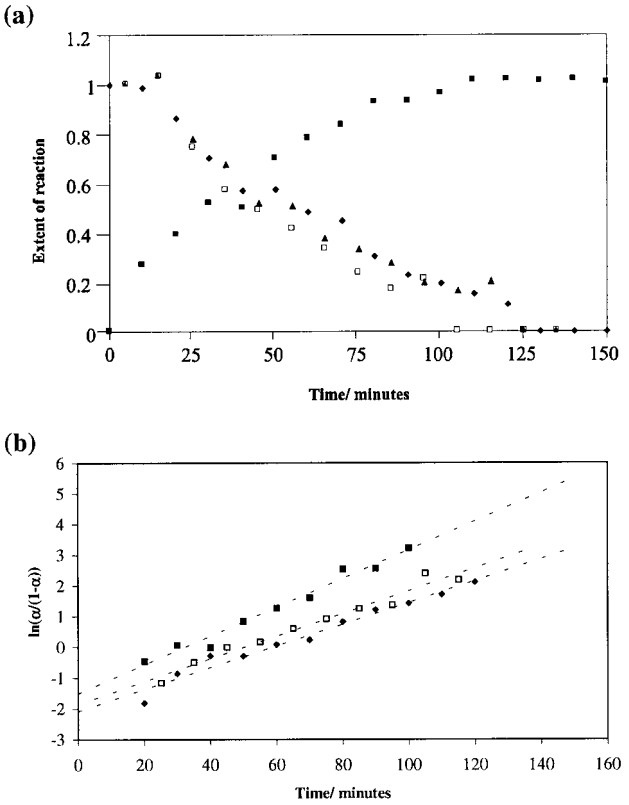

Figure 5. (a) Graphs of the area of the ammonium tetrathiomolybdate (202) [□] and (105) [▲] Bragg peaks normalized to unity for pure $(NH_4)_2MoS_4$, and the fractional coordination numbers of the Mo−S shells at 2.18[♦]and 2.45 Å [■] derived from XAFS coordination numbers for the thermal decomposition at 120 °C. (b) Plots of $\ln(\alpha/(1-\alpha))$ against time for the isothermal kinetic data determined from the XRD results (□), the change in EXAFS coordination number of the Mo−S shell at 2.45 Å (■), and the change in EXAFS coordination number of the Mo−S shell at 2.18 Å (♦). α has been scaled to represent the amount of remaining starting material in each case, to allow the graphs to be compared directly. Broken lines were fitted by linear regression; for the XRD data, $\ln(\alpha/(1-\alpha)) = 0.0396t - 1.8601$, for the change in long Mo−S distance observed by EXAFS, $\ln(\alpha/(1-\alpha)) = 0.0468t - 1.5142$, and for the short Mo−S distance, $\ln(\alpha/(1-\alpha)) = 0.0353t - 2.0776$.

diffraction data in the region of single well-resolved Bragg reflections. Although coordination numbers are difficult to obtain accurately from EXAFS, the general decrease in the proportion of the short Mo−S distance required to fit the EXAFS data closely follows the decrease in Bragg peak intensity of two reflections of ammonium tetrathiomolybdate. Also shown in Figure 5a is the change in the fractional amount of *a*-MoS_3 derived from the average EXAFS coordination number of the Mo−S correlation at 2.43 Å. It can be seen that the curves representing decay of starting material and growth of product intersect at close to 50%, consistent with the two-phase approach taken to modeling the EXAFS data.

The kinetics of thermal decompositions of the type A(solid) = B(solid) + C(gas) are complex and may comprise of up to five distinct stages of reaction, each described by a different mathematical expression.[44] A simple approach to modeling such kinetic data is to simulate the acceleratory period of reaction, where the largest physical changes are detectable and which often extends for the largest period of reaction. For the data determined here it was found that a simple exponential decay mechanism does not model the data well over any period of the reaction. However, the Prout−Tompkins equation ($\ln(\alpha/(1-\alpha)) = kt + C$, where α is the extent of reaction, the fractional amount of product formed, *k* a rate constant, and C a constant depending on the induction time of the process studied)[44] was found to model the kinetic data well over a large range of α and to produce consistent results between each data set. Figure 5b shows plots of $\ln(\alpha/(1-\alpha))$ against time for the combined, averaged XRD peak intensities and each of the two EXAFS derived kinetic curves for values of α between 0.25 and 0.95. It can be seen that each line has a similar gradient, therefore allowing an average rate constant to be determined of 0.040 min^{-1} for the acceleratory period of reaction. The differences in the intercept observed must arise from the fact that the induction time of the reaction, which has not been taken account of here, is very difficult to determine accurately from the XAFS results because of the large errors of EXAFS-derived coordination number. The Prout−Tompkins equation is entirely appropriate for the acceleratory period of a thermal decomposition reaction, originally being developed to describe the decomposition of potassium permanganate, and may be interpreted in terms of a mechanism involving the uniform growth of chains of product material which branch on encountering a crystal dislocation and terminate on mutual contact.[44] It must be borne in mind that when these results are compared with those from other experiments, solid-state decompositions often begin at lattice defects, and since sample damage by radiation is likely to occur when using X-ray methods as structural probes, decomposition may be enhanced, as has previously been shown for thermal processes.[45]

We now consider the EXAFS data of the sample of *a*-MoS_3 freshly prepared in situ. The data have so far only been fitted with two atomic shells, corresponding to sulfur near neighbors at 2.43 Å and molybdenum near neighbors at 2.77 Å. The refined coordination numbers of these shells show consistency with previous EXAFS studies of the compound. Structural models for *a*-MoS_3 in which molybdenum has close to six sulfur neighbors are most reasonable, and general agreement is found in the literature with this result.[24−31] The coordination number of the Mo−Mo shell at 2.77 Å ($N_{Mo} \approx 1.4$) is much more difficult to interpret and clearly does not exclusively favor models based on the Mo_2 dimer ($N_{Mo} = 1$) or the Mo_3 equilateral triangle ($N_{Mo} = 2$). It is worth noting that a previous study by Cramer et al. compared the EXAFS-derived Mo−Mo Debye−Waller factor for *a*-MoS_3 with those from model compounds containing Mo_3 and Mo_2 cores and concluded that Mo K edge EXAFS data favor the presence of dimer over trinuclear metal−metal bonded clusters in *a*-MoS_3.[26] Such a comparison was not performed here, but instead we use the EXAFS data of the freshly prepared *a*-MoS_3 to test the plausibility of other structural models

(44) Tompkins, F. C. Decomposition Reactions. In *Treatise on Solid State Chemistry*; Hannay, N. B., Ed.; Plenum Press: New York, 1976; Vol. 2, Chapter 2.

(45) Rao, C. N.; Gopalakrishan, J. *New Directions in Solid State Chemistry*, Cambridge University Press: Cambridge, U.K., 1997.

proposed. We found that including a third atomic shell (of Mo atoms) in the EXAFS model for *a*-MoS_3 produced no improvement in fit to the data. Some, but not all, of the previous EXAFS studies of *a*-MoS_3 suggest the presence of nonbonded Mo−Mo correlations at around 3.2 Å,[24−26] but if such a shell was added to the EXAFS data presented here, and least-squares refinements performed, a poorer fit resulted, with higher *R* factor (+1%) and high Debye−Waller factor (0.04 Å^2) for the third shell. Furthermore, if the third-shell occupation number was included in least-squares iterations, it refined to close to zero (0.02(3)) and the Debye−Waller factor became negative. This information allows one of the proposed structural building blocks of Weber et al. to be ruled out, namely, the Mo_3 cluster containing an Mo−Mo distance of ∼3 Å (Figure 1b). To the best of our knowledge, there exists no crystalline analogue of such a cluster in the extensive chemistry of the molybdenum−sulfur system, which makes such a trinuclear atomic arrangement of molybdenum atoms as a structural unit for *a*-MoS_3 even less plausible. It is noteworthy that a Mo−Mo bonded cluster has been prepared containing a Mo_2 dimer (d(Mo−Mo) = 2.80 Å) with a disulfide and a monosulfide anion bridging the metal pair, with a very similar atomic arrangement to that proposed for the Mo_2S_9 unit of the chain model for *a*-MoS_3.[46] We have not been able, using EXAFS, to unequivocally determine whether Mo−Mo bonded equilateral triangles or dimers, or a mixture of both, best describes the structure of *a*-MoS_3. If, as we believe, the chain model best describes the structure of *a*-MoS_3, then short nonbonded Mo−Mo correlations must be present in the structure of around 3−3.5 Å, between Mo atoms of neighboring Mo_2S_9 units. The fact that the EXAFS data of the compound show no evidence for the presence of a single distance within this range suggests that there is a large amount of static disorder associated with the correlation; i.e. there exists a range of Mo−Mo short nonbonded distances. This suggests that in *a*-MoS_3 great disorder exists beyond the simple Mo_2S_9 unit, explaining why the material is amorphous. A likely explanation for the past observation of Mo−Mo correlations at ∼3.2 Å in *a*-MoS_3 will be given below when the decomposition of *a*-MoS_3 into MoS_2 is considered.

Decomposition of Ammonium Tetrathiomolybdate with Increasing Temperature. The powder diffraction data, collected as a sample of ammonium tetrathiomolybdate heated to 100−400 °C with a temperature rate of 1 °C min^{-1}, showed the decomposition of the crystalline starting material was complete after heating to 150 °C, i.e. after 50 min of heating. On continued heating of the product under the same temperature ramp, broad features around $2\theta \sim 24-27°$ and $2\theta \sim 42-47°$ appeared when the temperature had attained 300 °C, and these became more intense on continued heating to 400 °C. Figure 6 shows the powder pattern of the material collected at three different times, along with data collected from crystalline hexagonal MoS_2 at 400 °C. The data measured here from the decomposition product of ammonium tetrathiomolybdate at 400 °C are very similar to diffraction data collected by other workers from samples of poorly crystalline MoS_2 prepared by a similar route[9,14] and

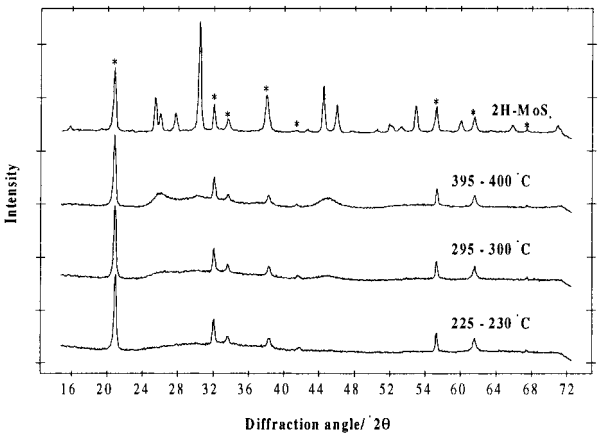

Figure 6. Selected powder diffraction patterns recorded as the amorphous decomposition products of ammonium tetrathiomolybdate heated under a temperature gradient of 1 °C min^{-1} compared with the pattern of hexagonal MoS_2. Bragg peaks marked an asterisk are due to crystalline boron nitride, the diluent.

Table 2. Structural Parameters Derived from Study of the Mo K Edge EXAFS Obtained during the Heating of $(NH_4)_2MoS_4$ from 100 to 400 °C under a temperature rate of 1 °C min^{-1} at Selected Temperatures (Legend as for Table 1)

temp/°C	shell	*N*	*R*/Å	*A*/Å^2	fit index
280−285	S	5.99(15)	2.418(2)	0.0168(5)	2.26
	Mo	1.56(19)	2.750(3)	0.0154(12)	
300−305	S	5.13(14)	2.409(2)	0.0128(4)	2.00
	Mo	1.28(30)	2.741(6)	0.0194(28)	
	Mo	1.61(24)	3.147(3)	0.0128(14)	
320−325	S	5.25(14)	2.401(1)	0.0110(3)	1.91
	Mo	0.25(13)	2.764(7)	0.0067(37)	
	Mo	2.53(27)	3.1478(2)	0.0117(9)	
340−345	S	5.53(14)	2.402(1)	0.0114(3)	1.81
	Mo	0.09(9)	2.764(10)	0.0029(63)	
	Mo	3.56(33)	3.151(2)	0.0142(9)	
360−355	S	5.79(90)	2.403(2)	0.0116(4)	3.18
	Mo	3.30(45)	3.254(3)	0.0159(1)	
380−385	S	5.57(16)	2.401(2)	0.0115(4)	2.43
	Mo	3.02(37)	3.153(2)	0.0155(10)	

illustrate the highly disordered nature of the material. Elemental analysis of the decomposition product after cooling showed it to have composition $MoS_{1.9(1)}$.

EXAFS data collected alternately with the diffraction data were analyzed using an approach similar to the data analysis described in the previous section. For the conversion of ammonium tetrathiomolybdate to *a*-MoS_3 very similar results were obtained; i.e. every EXAFS spectrum could be interpreted as arising from a mixture of ammonium tetrathiomolybdate and *a*-MoS_3 with increasing amounts of *a*-MoS_3 in the mixture with increasing time and temperature. Once the temperature had reached 150 °C, the data could be modeled as arising from only *a*-MoS_3 and very similar structural parameters to those derived in the first experiment were obtained. The simple model of two atomic shells fits the EXAFS data well until a temperature of 290 °C is reached, when a third shell of atoms is necessary to produce a satisfactory fit to the data. Fixing this shell to contain Mo atoms at ∼3.2 Å and performing least-squares refinements of all structural parameters produces the model shown in Table 2. The refined Mo−Mo distance of 3.15 Å agrees closely with the shortest Mo−Mo nonbonded distance of 3.16 Å observed crys-

(46) Coffey, T.; Hogarth, G. *Polyhedron* **1997**, *16*, 165.

tallographically in 2H−MoS_2[47] and is consistent with the fact that the X-ray powder pattern collected at the time closest to these EXAFS data (295−300 °C, Figure 6) exhibits the diffuse features which develop into the broad "Bragg reflections" of poorly crystalline MoS_2. It should be noted that in 2H−MoS_2 each molybdenum has six sulfur neighbors at 2.42 Å, so the first near-neighbor shell of Mo during the transformation of *a*-MoS_3 to MoS_2 will change very little.

The current experiment shows that when only very diffuse features due to poorly crystalline MoS_2 are seen in the diffraction pattern of the product mixture of ammonium tetrathiomolybdate decomposition, an Mo−Mo correlation at ∼3.2 Å may be observed by EXAFS. This strongly suggests that the Mo−Mo distance of 3.2 Å observed by some previous workers in *a*-MoS_3 may arise from the presence of contaminant poorly crystalline MoS_2, which is difficult to detect by X-ray powder diffraction.

The ten EXAFS data sets collected between 300 and 400 °C could be analyzed in exactly the same manner as mixtures of *a*-MoS_3 and MoS_2 with decreasing amounts of *a*-MoS_3 in the product mixture (less contribution of the short Mo−Mo distance at 2.77 Å) and increasing amounts of poorly crystalline MoS_2 present. As with the first step of the thermal decomposition of ammonium tetrathiomolybdate, there is no evidence for the presence of any intermediates of differing local structure than *a*-MoS_3 or MoS_2. Table 2 contains the results of least-squares refinements of all parameters of all atomic shells for representative EXAFS scans. Figure 7 shows the Mo K edge EXAFS spectra at various temperatures along with that of 2H−MoS_2 at 400 °C.

The EXAFS data of poorly crystalline MoS_2 prepared in situ differ from those collected from 2H−MoS_2 at 400 °C (Figures 7b, c). Least-squares refinements of structural parameters modeling these data (Table 3) show that the major structural difference between the materials is associated with the second coordination shell of molybdenum, where a noticeably different shell occupation number and Debye−Waller factor are obtained. Interpretation of these parameters as they stand is problematic because of the correlation of shell occupation numbers with Debye−Waller factors. To gain further insight into the significance of these results, we fixed the first-shell (Mo−S) structural parameters at values obtained by initial least-squares refinement and calculated contour maps showing the effect on the fit index of the second shell Debye−Waller factor and occupation number. Figure 8 shows the results for 2H−MoS_2 at a variety of temperatures between ambient and 400 °C and for poorly crystalline MoS_2 as prepared in situ and after cooling to room temperature. It can clearly be seen that for 2H−MoS_2 as the temperature is raised the largest effect on the structural parameters of the Mo shell is an increase in the Debye−Waller factor, reflecting the increase in thermal disorder in the material, and that the Mo−Mo coordination number remains approximately constant around 6 (consistent with the crystal structure of the compound). For poorly crystalline MoS_2, at the two temperatures at which EXAFS data were obtained, the Mo−Mo coordination

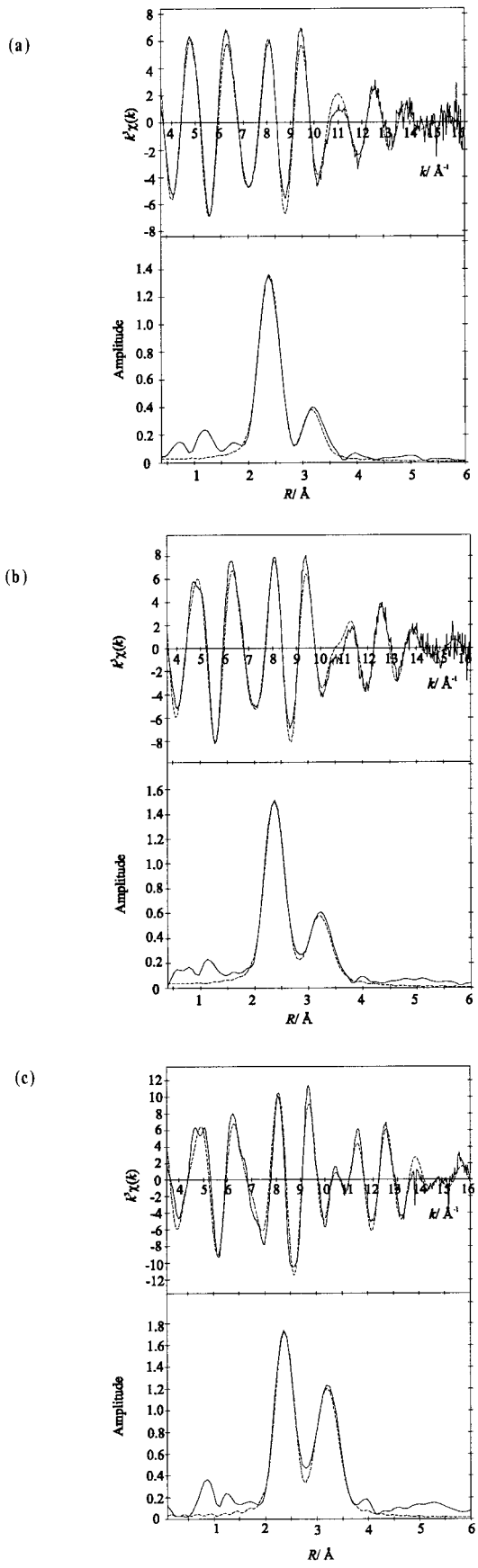

Figure 7. Mo K edge EXAFS spectra (top) with their Fourier transforms (bottom) recorded during the heating of ammonium tetrathiomolybdate at 1 °C min^{-1} at (a) 300−305 and (b) 395−400 °C and for (c) 2H−MoS_2 at 400 °C. Line convention as for Figure 3.

(47) Bosema, K. D.; De Boer, J. L.; Jellinek, F. *Z. Anorg. Allg. Chem.* **1986**, *540*, 15.

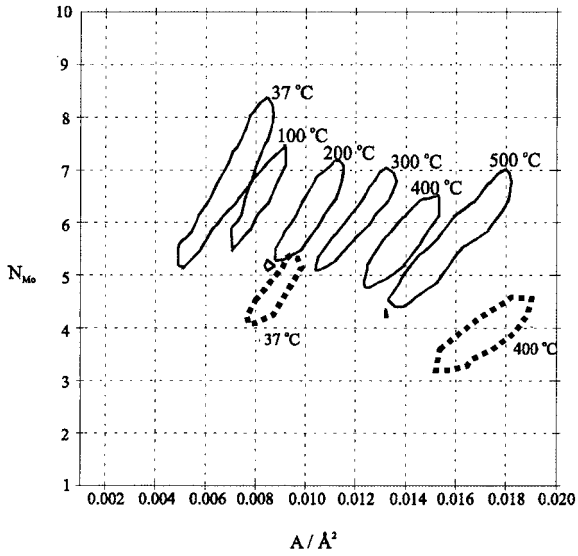

Figure 8. Variation of the second shell coordination number (N_{Mo}) with Debye−Waller factor (A) for crystalline 2H−MoS_2 (full line) and poorly crystalline MoS_2 (broken line). The bold contour indicates the area within which the two parameters lie to 95% probability.

Table 3. Comparison of the Mo K Edge Derived Structural Parameters of Poorly Crystalline (*pc*) MoS_2 Freshly Prepared in Situ at 390−395 °C with Those of Crystalline 2H−MoS_2 at 400 °C (Legend as for Table 1)

compd	shell	N	R/Å	A/Å²	fit index
pc-MoS_2	S	5.10(11)	2.404(1)	0.0115(4)	1.70
	Mo	3.21(28)	3.157(2)	0.0155(10)	
2H−MoS_2	S	6.09(18)	2.404(2)	0.00911(2)	2.64
	Mo	5.56(43)	3.167(2)	0.0126(2)	

number is lower and the Debye−Waller factor higher than for crystalline MoS_2.

Small particle size clearly contributes to a large part of the disorder in poorly crystalline MoS_2, as evidenced by the lower than expected coordination number for the Mo−Mo shell, 4−5, instead of 6 in 2H−MoS_2. Assuming small particles of MoS_2 may be made up of hexagonal slabs of 2H−MoS_2 bounded by sulfur atoms (to retain average Mo−S coordination number), an estimated particle size for a given Mo−Mo coordination number may be determined using simple geometry. An Mo−Mo coordination number of 4.8 is produced for hexagonal particles with edges of five sulfur atoms which correspond to a hexagon edge of ∼15.8 Å. Such particles will therefore have a maximum dimension of ∼30 Å (the "diameter of the hexagon"). It should be noted that these values are independent of particle thickness. Slabs can be stacked to form a more extended structure, but EXAFS yields no information on this third dimension. The calculated particle size is appropriate for the poorly crystalline material studied here, which exhibits an Mo−Mo coordination number of ∼4.5 (Figure 8) and shows good agreement with the value of 30 Å, suggested by Liang et al. for the size of particles of pc-MoS_2 on the basis of their X-ray diffraction study.[14]

Table 3 shows clearly that the Debye−Waller factor of the Mo−S correlation in pc-MoS_2 is very similar to that observed in 2H−MoS_2, both being very close to 0.01 Å², and this is consistent with the model suggested above in which the local coordination of Mo in pc-MoS_2 is identical to that of Mo in 2H−MoS_2. The contour map, Figure 8, highlights the fact that the Mo−Mo correlation in pc-MoS_2 has associated with it static disorder, not present in 2H−MoS_2, where Mo is surrounded by six other equidistant Mo atoms.[47] This static disorder (∼0.003 Å²) in part contributes to the disorder of pc-MoS_2.

Acknowledgment. We thank the Engineering and Physical Sciences Research Council (EPSRC, U.K.) for a studentship (R.I.W.) and for provision of facilities at Daresbury Laboratory.

Supporting Information Available: Tables of EXAFS-derived structural parameters from analysis of each EXAFS spectrum measured during the thermal decomposition experiments (2 pages). Ordering information is given on any current masthead page.

CM980716H